Parallel Particle-In-Cell Simulation of High Intensity Beams

Ji Qiang

Lawrence Berkeley National Laboratory

22nd International Conference on Numerical Simulation of Plasmas , September 7-9, Long Branch, NJ, USA

High-resolution multi-physics particle-in-cell simulation is required for state-of-the-art accelerator design

For example

- The microbunching instability significantly degrades beam quality
- Halo particles generated through accelerator could cause uncontrolled particle loss and machine radiation
- High resolution modeling is needed to accurately model initial shot noise, resolve fine structure, and avoid numerical artifacts

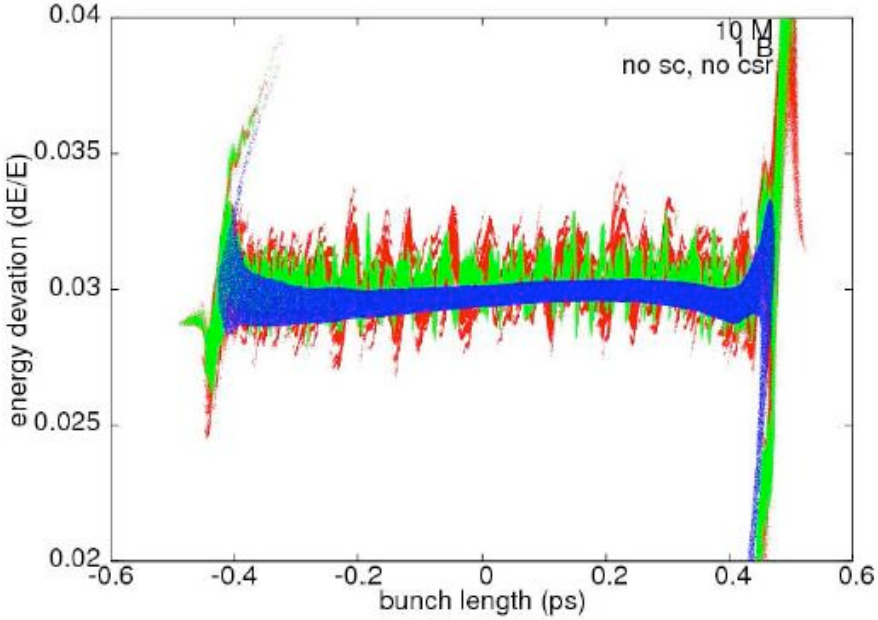

The longitudinal phase space of a beam at the exit of a linac

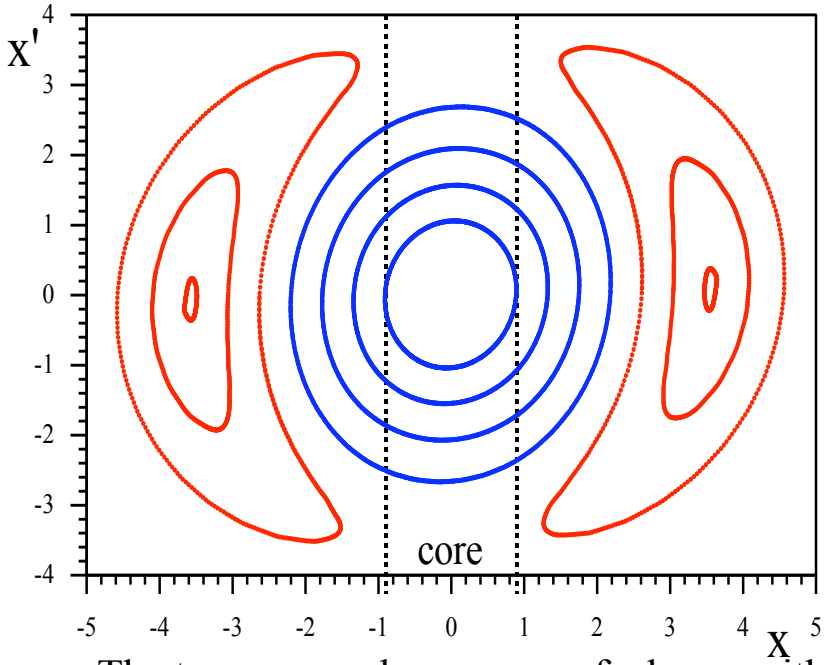

The transverse phase space of a beam with initial mismatch

Particle-In-Cell Simulation with Split-Operator Method

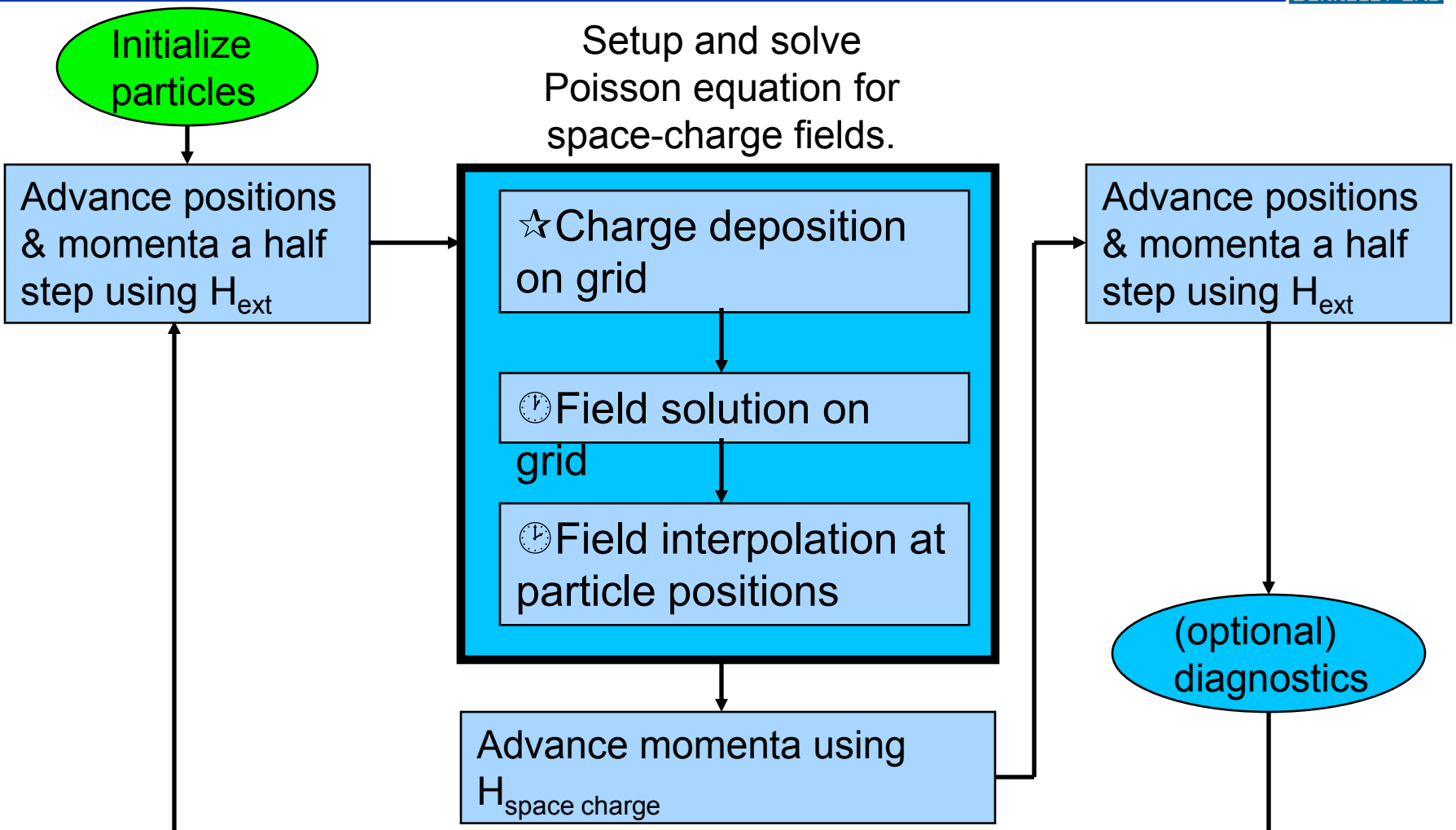

- Rapidly varying s-dependence of external fields is decoupled from slowly varying space charge fields
- Leads to very efficient particle advance:
  - Do not take tiny steps to push millions - billions of particles
  - Do take tiny steps to compute maps; then push particles w/ maps

Linear Transfer Maps in an Acceleration Structure for Momentum Advancement

$$\begin{pmatrix} \bar{x} \\ \bar{p}_x \end{pmatrix}^f = \begin{pmatrix} u^{-1/2} & 0 \\ -u^{1/2}\Delta & u^{1/2} \end{pmatrix}^f \begin{pmatrix} a_x & b_x \\ c_x & d_x \end{pmatrix}^f \begin{pmatrix} u^{1/2} & 0 \\ u^{1/2}\Delta & u^{-1/2} \end{pmatrix}^i \begin{pmatrix} \bar{x} \\ \bar{p}_x \end{pmatrix}^i$$

$$\begin{pmatrix} \bar{y} \\ \bar{p}_y \end{pmatrix}^f = \begin{pmatrix} u^{-1/2} & 0 \\ -u^{1/2}\Delta & u^{1/2} \end{pmatrix}^f \begin{pmatrix} a_y & b_y \\ c_y & d_y \end{pmatrix}^f \begin{pmatrix} u^{1/2} & 0 \\ u^{1/2}\Delta & u^{-1/2} \end{pmatrix}^i \begin{pmatrix} \bar{y} \\ \bar{p}_y \end{pmatrix}^i$$

$$\begin{pmatrix} \phi \\ \bar{p}_t \end{pmatrix}^f = \begin{pmatrix} u^{-3/2} & 0 \\ -\frac{3l}{2}\left(\frac{u'}{u}\right)u^{3/2} & u^{3/2} \end{pmatrix}^f \begin{pmatrix} a_\phi & b_\phi \\ c_\phi & d_\phi \end{pmatrix}^f \begin{pmatrix} u^{3/2} & 0 \\ \frac{3l}{2}\left(\frac{u'}{u}\right)u^{3/2} & u^{-3/2} \end{pmatrix}^i \begin{pmatrix} \phi \\ \bar{p}_t \end{pmatrix}^i,$$

$$\Delta = \frac{l}{2}\left[\frac{(\beta_0\gamma_0)'}{\beta_0\gamma_0} - \frac{(q/mc^2)\varepsilon'\sin(\phi_s)}{\beta_0\gamma_0\omega_\alpha/c}\right] \qquad (12)$$

and $u = \gamma_0\beta_0,\ l = c/\omega,\ \beta_0 = v_{z0}/c,\ \gamma_0 = 1/\sqrt{1-\beta_0^2},$

$$a'_j = c_j/l, \qquad b'_j = d_j/l,$$

$$c'_j = -l\Omega_j a_j, \qquad d'_j = -l\Omega_j b_j$$

$$t'_0 = \frac{\gamma_0/c}{\sqrt{\gamma_0^2 - 1}} \qquad (13)$$

$$\gamma'_0 = (q/mc^2)\varepsilon(z)\cos(\omega_\alpha t_0 + \theta). \qquad (14)$$

$$\Omega_x = \Omega_y = \frac{(q/mc^2)(\omega_\alpha/c)}{2\beta_0^3\gamma_0^3}\varepsilon\sin(\phi_s) + \frac{1}{2}\left(1 + \frac{\gamma_0^2}{2}\right)\left(\frac{(q/mc^2)\varepsilon\cos(\phi_s)}{\beta_0^2\gamma_0^2}\right)^2$$

$$\Omega_\phi = \frac{\beta_0^2 + \frac{1}{2}}{\beta_0^3\gamma_0}(q/mc^2)(\omega_\alpha/c)\varepsilon\sin(\phi_s) - \frac{3}{2}\frac{q/mc^2}{\beta_0^2\gamma_0}\varepsilon'\cos(\phi_s) + \frac{3}{2}\left(1 - \frac{\gamma_0^2}{2}\right)\left(\frac{(q/mc^2)\varepsilon\cos(\phi_s)}{\beta_0^2\gamma_0^2}\right)^2.$$

R. D. Ryne, Los Alamos National Laboratory Technical Report, 1995.

Green Function Solution of Poisson's Equation (open boundary conditions)

$$\phi(r) = \int G(r, r')\rho(r')dr' \; ; \quad r = (x, y, z)$$

$$\phi(r_i) = h\sum_{i'=1}^{N} G(r_i - r_{i'})\rho(r_{i'})$$

$$\boxed{G(x, y, z) = 1/\sqrt{(x^2 + y^2 + z^2)}}$$

Direct summation of the convolution scales as N^6 !!!!
N – grid number in each dimension

Hockney's Algorithm /zero padding:- *scales as $(2N)^3 \log(2N)$*

- Ref: Hockney and Easwood, *Computer Simulation using Particles*, McGraw-Hill Book Company, New York, 1985.

$$\phi_c(r_i) = h\sum_{i'=1}^{2N} G_c(r_i - r_{i'})\rho_c(r_{i'})$$

$$\phi(r_i) = \phi_c(r_i) \quad \text{for i} \; = \; 1, \text{N}$$

Integrated Green Function Solution of Poisson's Equation (large aspect ratio beam with open boundary conditions)

$$_c(r_i) = \sum_{i'=1}^{2N} G_i(r_i \quad r_{i'}) \quad _c(r_{i'})$$

$$G_i(r,r') = \circ G_s(r,r')\,dr'$$

integrated Green function

$$G_s(x,y,z) = 1/\sqrt{(x^2+y^2+z^2)}$$

standard Green function

Integrated Green's function is needed for modeling large aspect ratio beams!

(O(N log N))

Comparison between the IG and SG for a beam with aspect ratio of 30

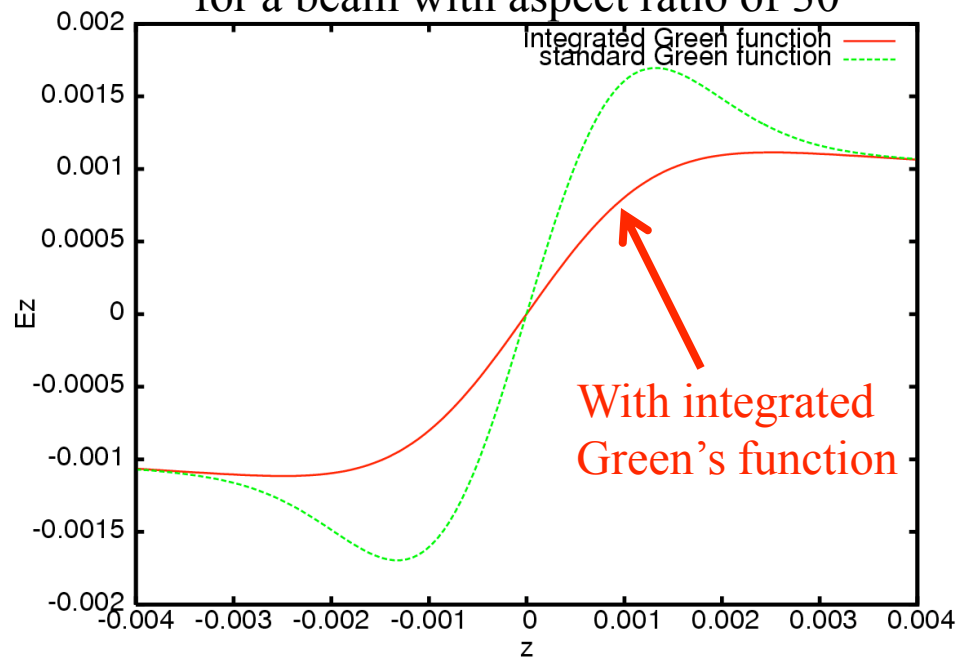

R. D. Ryne, ICFA Beam DynamicsMini Workshop on Space Charge Simulation, Trinity College, Oxford, 2003

J. Qiang, S. Lidia, R. D. Ryne, and C. Limborg-Deprey, Phys. Rev. ST Accel. Beams, vol 9, 044204 (2006).

Efficient Shifted Green Function Method to Calculate Image Space-Charge Effects

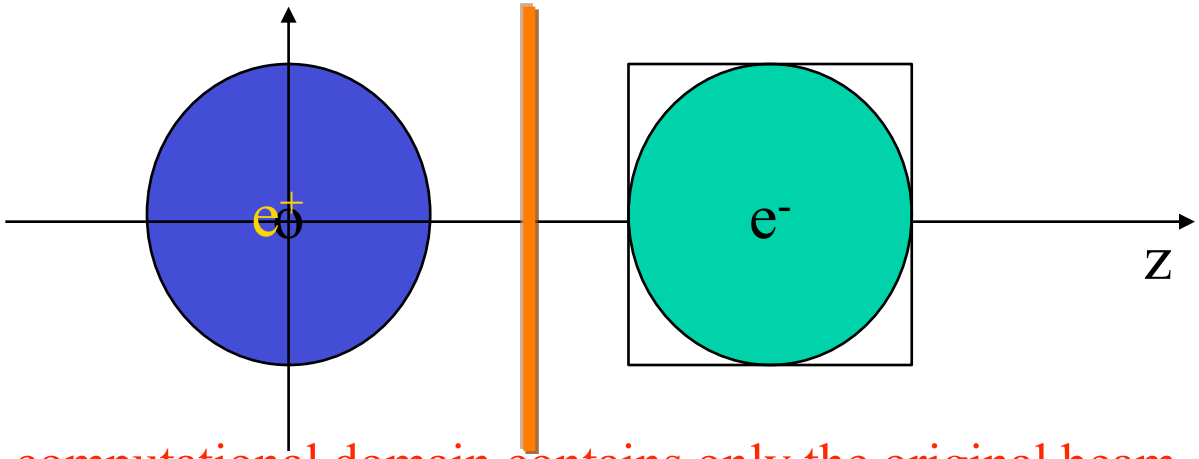

computational domain contains only the original beam

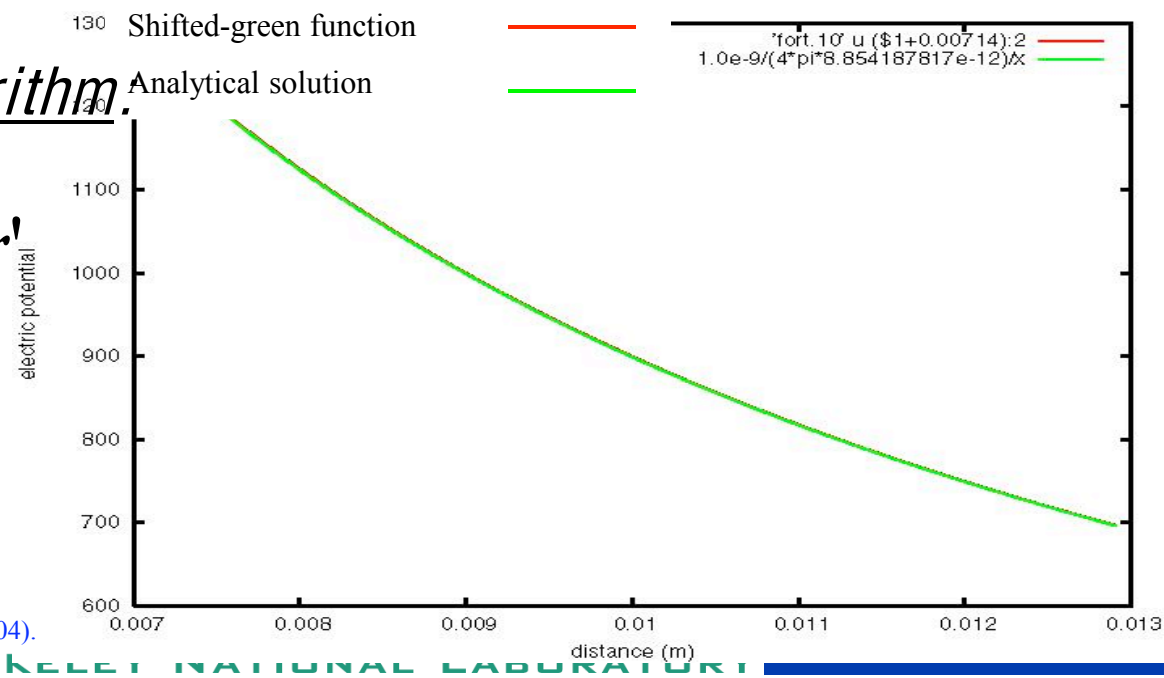

Shifted Green function Algorithm:

$$\phi_F(r) = \int G_s(r,r')\rho(r')dr'$$

$$G_s(r,r') = G(r + r_s, r')$$

(O(N logN))

J. Qiang, M. Furman, and R. Ryne, J. Comp. Phys. vol. 198, 278 (2004).

3D Poisson Solver with Transverse Rectangular Pipe

$$\frac{\partial^2\phi}{\partial x^2}+\frac{\partial^2\phi}{\partial y^2}+\frac{\partial^2\phi}{\partial z^2}=-\frac{\rho}{\epsilon_0}$$

with boundary conditions

$$\begin{aligned}\phi(x=0,y,z) &= 0,\\ \phi(x=a,y,z) &= 0,\\ \phi(x,y=0,z) &= 0,\\ \phi(x,y=b,z) &= 0,\\ \phi(x,y,z=\pm\infty) &= 0,\end{aligned}$$

$$\rho(x,y,z)=\sum_{l=1}^{N_l}\sum_{m=1}^{N_m}\rho^{lm}(z)\sin(\alpha_l x)\sin(\beta_m y),$$

$$\phi(x,y,z)=\sum_{l=1}^{N_l}\sum_{m=1}^{N_m}\phi^{lm}(z)\sin(\alpha_l x)\sin(\beta_m y),$$

where

$$\rho^{lm}(z)=\frac{4}{ab}\int_0^a\int_0^b\rho(x,y,z)\sin(\alpha_l x)\sin(\beta_m y),$$

$$\phi^{lm}(z)=\frac{4}{ab}\int_0^a\int_0^b\phi(x,y,z)\sin(\alpha_l x)\sin(\beta_m y),$$

$$\frac{\partial^2\phi^{lm}(z)}{\partial z^2}-\gamma_{lm}^2\phi^{lm}(z)=-\frac{\rho^{lm}(z)}{\epsilon_0},$$

$$\frac{\phi_{n+1}^{lm}-2\phi_n^{lm}+\phi_{n-1}^{lm}}{h_z^2}-\gamma_{lm}^2\phi_n^{lm}=-\frac{\rho_n^{lm}}{\epsilon_0},$$

$$\begin{aligned}\phi_{-1}^{lm}&=\exp(-\gamma_{lm}h_z)\phi_0^{lm}, &\quad n=0,\\ \phi_{N+1}^{lm}&=\exp(-\gamma_{lm}h_z)\phi_N^{lm}, &\quad n=N.\end{aligned}$$

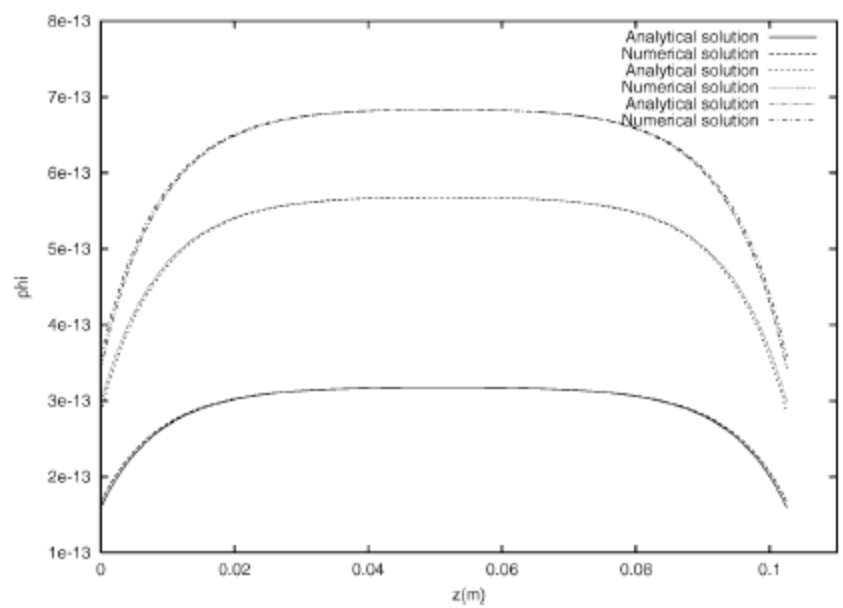

J. Qiang, and R. Ryne, Comput. Phys. Comm. 138, p. 18 (2001).

3D Poisson Solver inside a Ring

$$\nabla_\perp^2\phi + \frac{1}{R}\frac{1}{1+\frac{r\cos(\theta)}{R}}\left(\cos(\theta)\frac{\partial\phi}{\partial r} - \frac{\sin(\theta)}{r}\frac{\partial\phi}{\partial r}\right) + \frac{1}{\left(1+\frac{r\cos(\theta)}{R}\right)^2}\frac{\partial^2\phi}{\partial z^2} = -\rho.$$

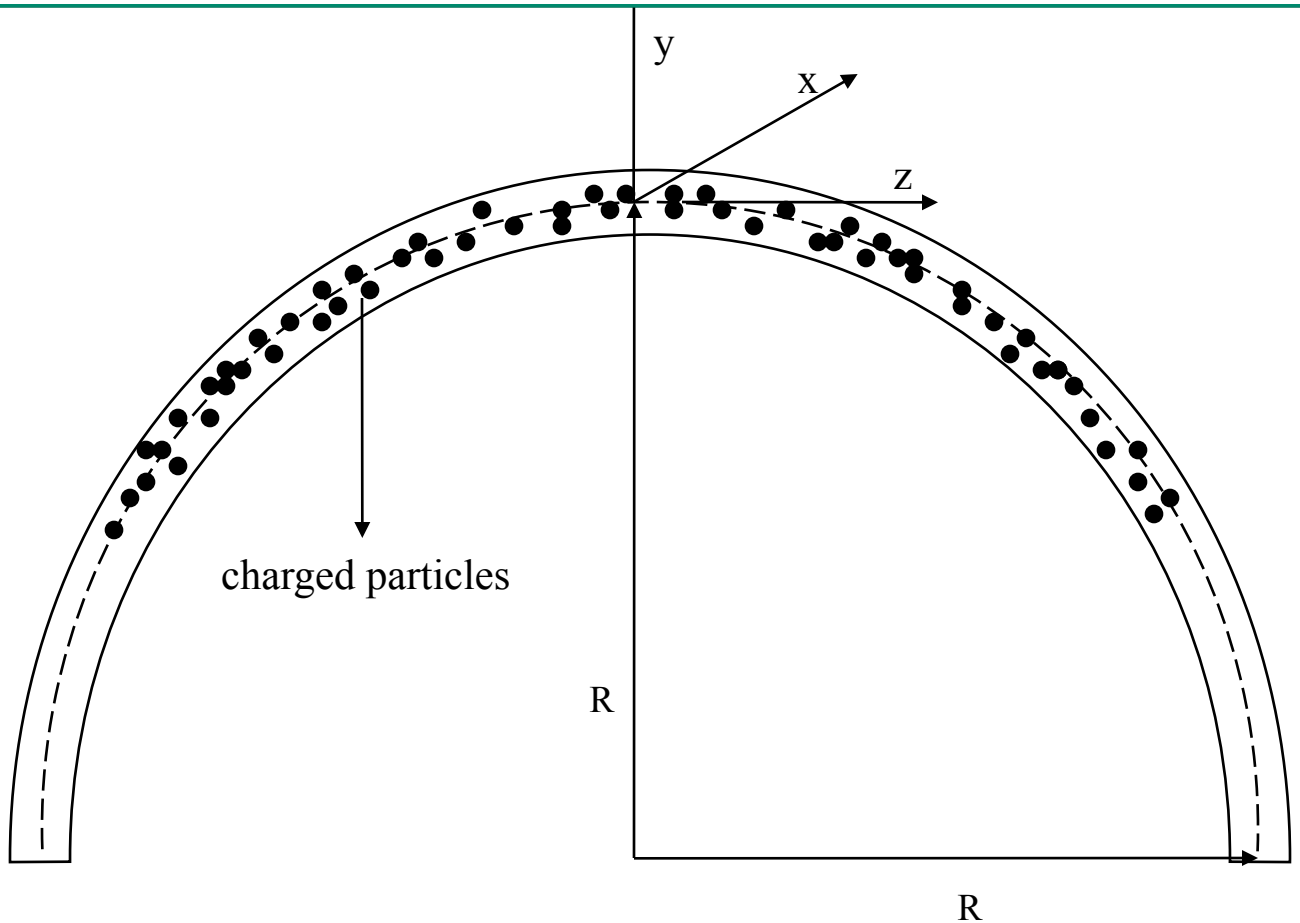

J. Qiang, and R. L. Gluckstern, Comput. Phys. Comm. 160, p. 120 (2004).

Iterative Solution of the Poisson Equation with the Hermite-Gaussian Approximation

$$\rho(r,\theta,z) = \sum_{n=0}^{N} \rho_n(r,\theta)\mathcal{H}_n(z),$$

$$\phi(r,\theta,z) = \sum_{n=0}^{N} \phi_n(r,\theta)\mathcal{H}_n(z).$$

$$\mathcal{H}_n(z) = H_n\left(\frac{z}{A}\right)\exp\left(-\frac{1}{2}\frac{z^2}{A^2}\right)$$

$$\nabla_\perp^2\phi_n + \frac{1}{R}\frac{1}{1+\frac{r\cos(\theta)}{R}}\left(\cos(\theta)\frac{\partial\phi_n}{\partial r} - \frac{\sin(\theta)}{r}\frac{\partial\phi_n}{\partial r}\right)$$
$$+ \frac{1}{\left(1+\frac{r\cos(\theta)}{R}\right)^2}\left(\frac{1}{4}\phi_{n-2} - \frac{1}{2}(2n+1)\phi_n + (n+2)(n+1)\phi_{n+2}\right)\frac{1}{A^2} = -\rho_n.$$

$$\nabla_\perp^2\phi_n^1 = -\rho_n,$$
$$\nabla_\perp^2\phi_n^2 = -\rho_n - \frac{1}{R}\frac{1}{1+\frac{r\cos(\theta)}{R}}\left(\cos(\theta)\frac{\partial\phi_n^1}{\partial r} - \frac{\sin(\theta)}{r}\frac{\partial\phi_n^1}{\partial r}\right)$$
$$+ \left(\frac{1}{4}\phi_{n-2}^1 - \frac{1}{2}(2n+1)\phi_n^1 + (n+2)(n+1)\phi_{n+2}^1\right)\frac{1}{\left(1+\frac{r\cos(\theta)}{R}\right)^2}\frac{1}{A^2},$$
$$\nabla_\perp^2\phi_n^3 = -\rho_n - \frac{1}{R}\frac{1}{1+\frac{r\cos(\theta)}{R}}\left(\cos(\theta)\frac{\partial\phi_n^2}{\partial r} - \frac{\sin(\theta)}{r}\frac{\partial\phi_n^2}{\partial r}\right)$$
$$+ \left(\frac{1}{4}\phi_{n-2}^2 - \frac{1}{2}(2n+1)\phi_n^2 + (n+2)(n+1)\phi_{n+2}^2\right)\frac{1}{\left(1+\frac{r\cos(\theta)}{R}\right)^2}\frac{1}{A^2},$$
$$\vdots = \vdots.$$

An Electric Potential and Convergence

Potential of a beam in a toroidal conducting pipe (aspect ratio = 100)

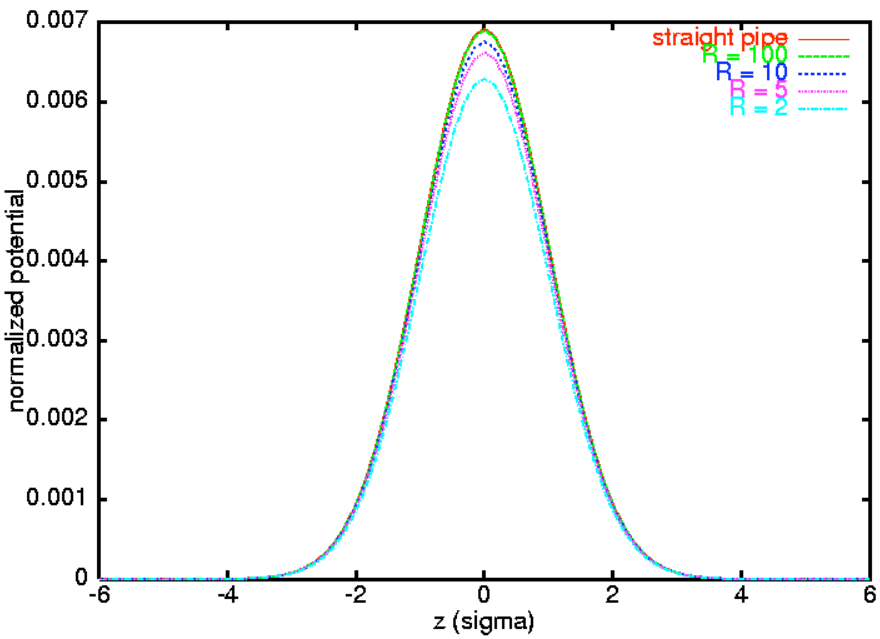

Norm 1 Errors vs. Number of Iterations

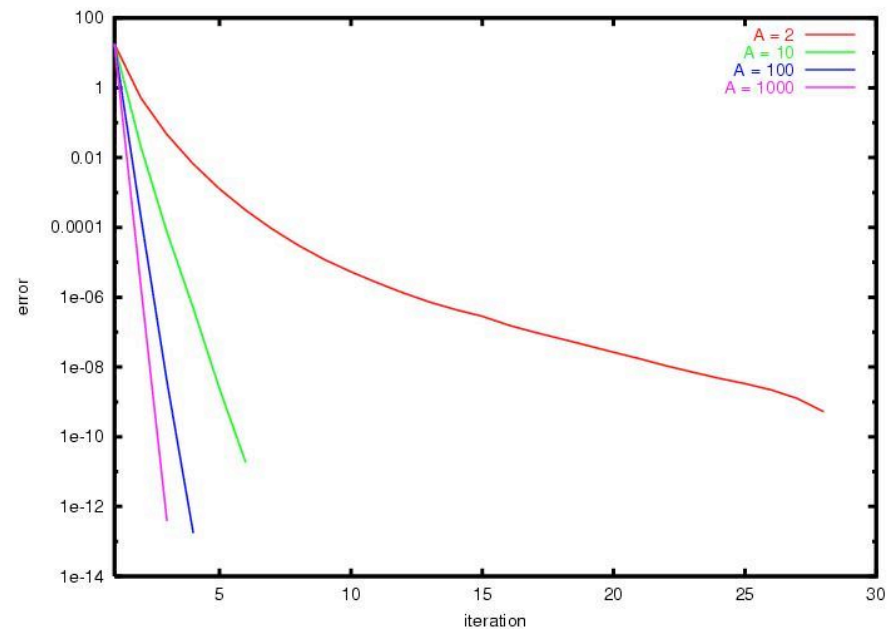

Parallel Implementation

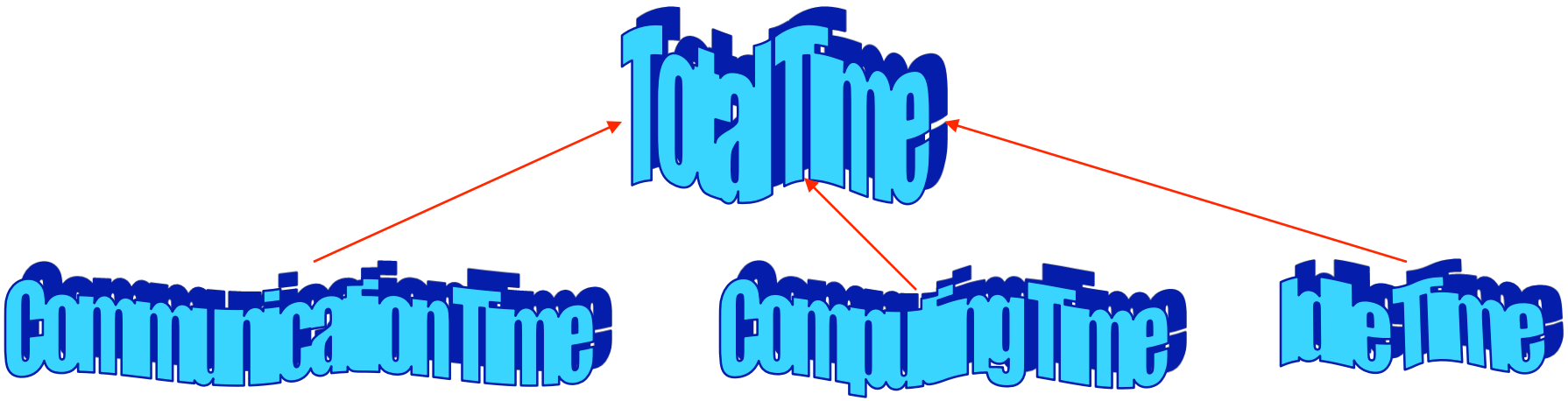

- Parallel Implementation of PIC Simulation
  - Particle decomposition
  - Domain decomposition
  - Particle-field decomposition

Particle Decomposition

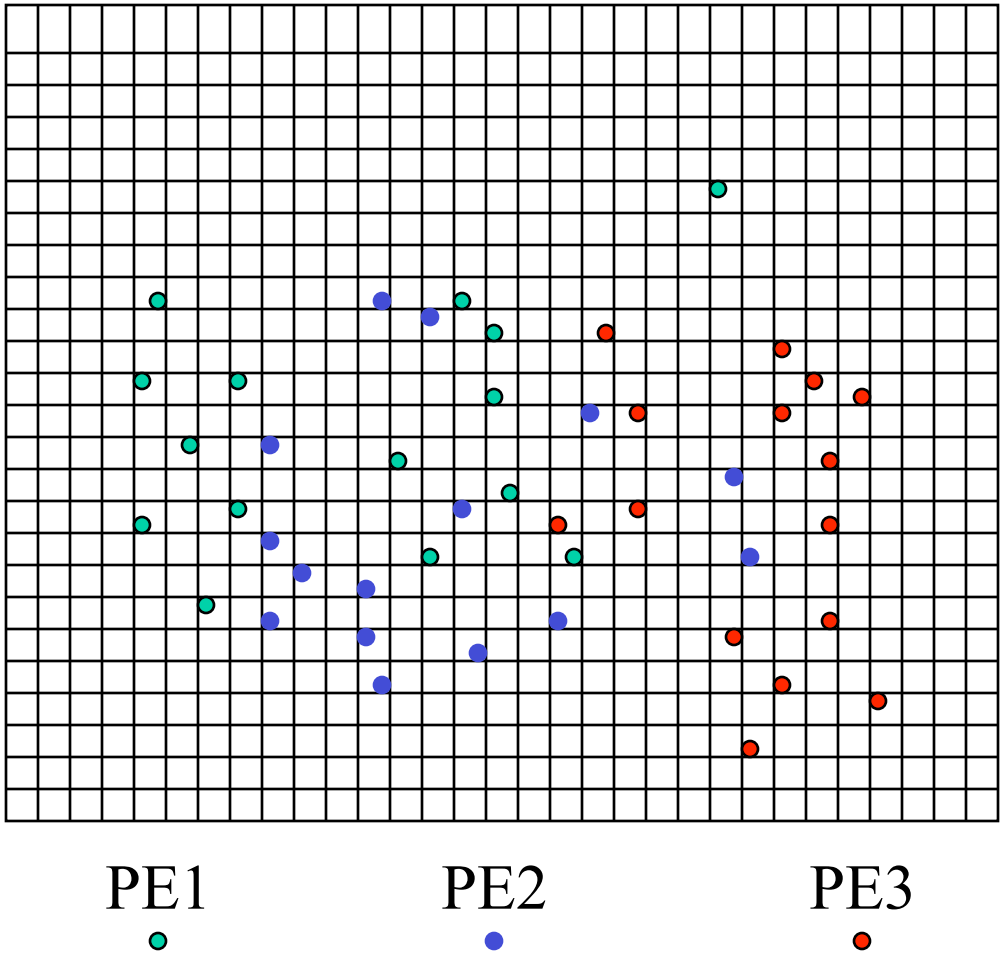

Domain Decomposition

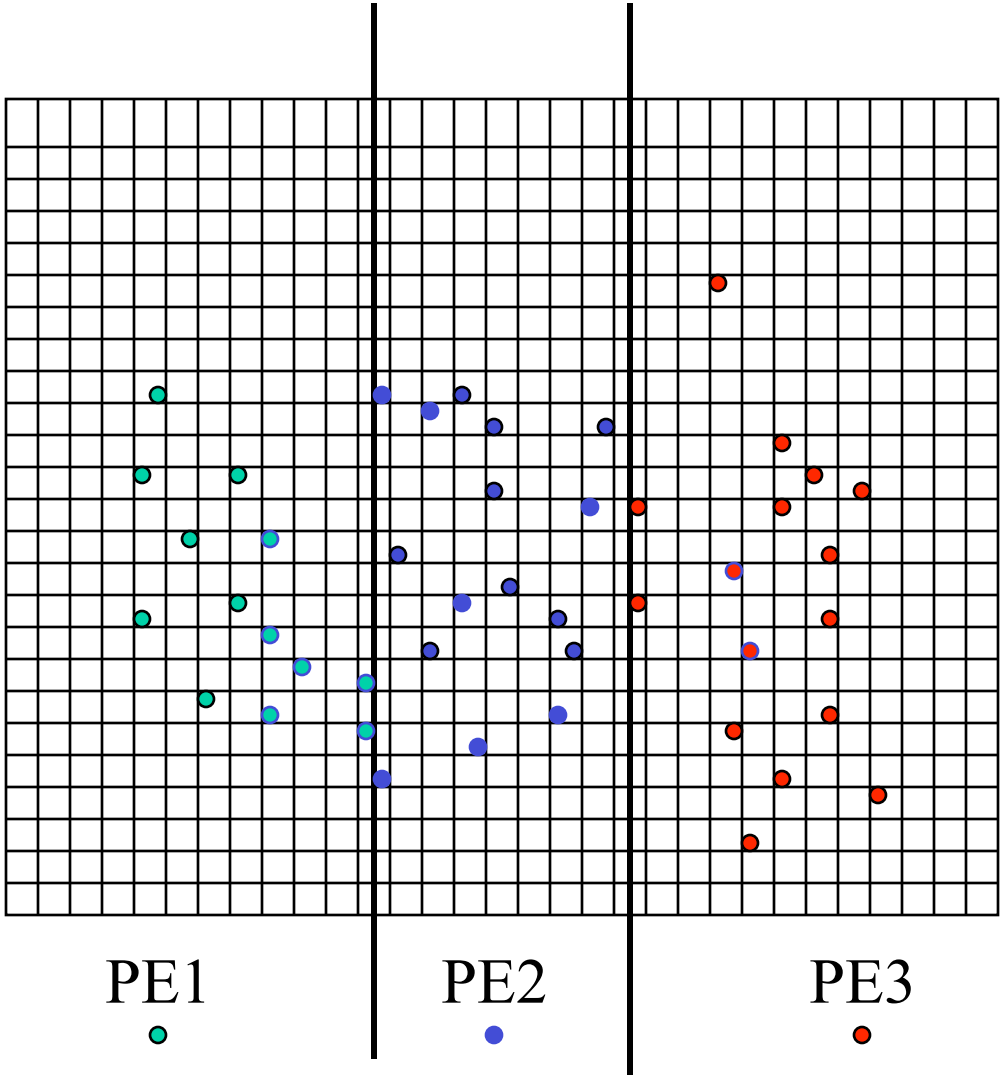

Particle-Field Decomposition

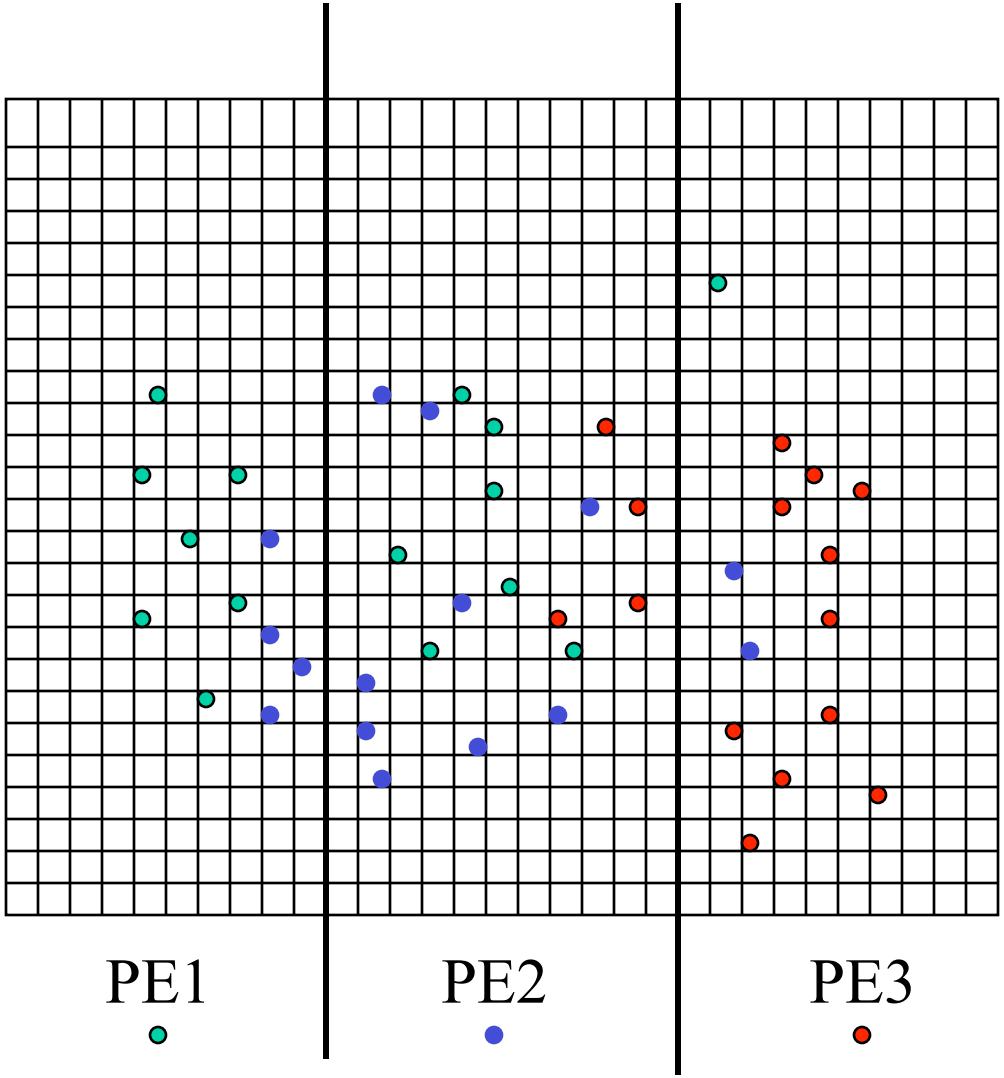

Scalability with large number of macroparticles (500) per cell

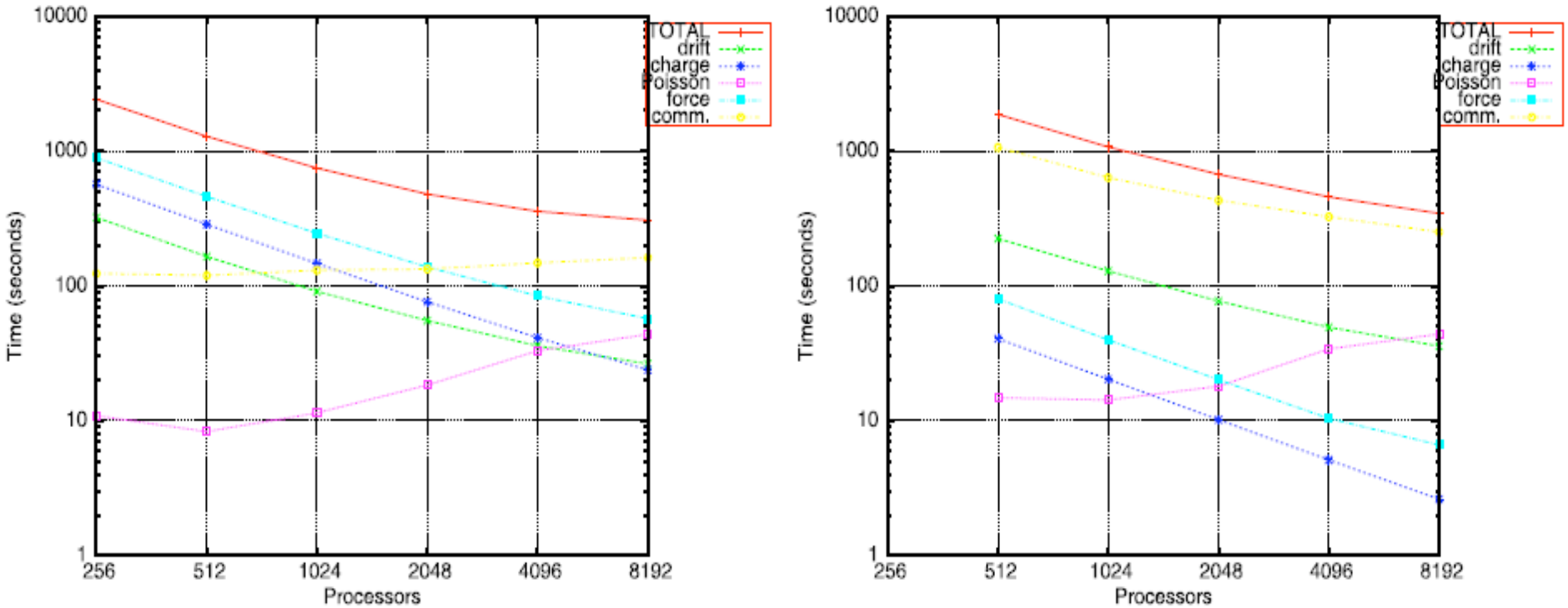

Fig. 5. Computing time as a function of number of processors on Cray XT4 using the particle-field decomposition scheme (left) and the domain decomposition scheme (right) in the strong scaling test A with $32 \times 32 \times 2048$ grid points and 1 billion particles.

J. Qiang and X. Li, Comput. Phys. Comm., 181, 2024, (2010).

Scalability with small number of macroparticles (5) per cell

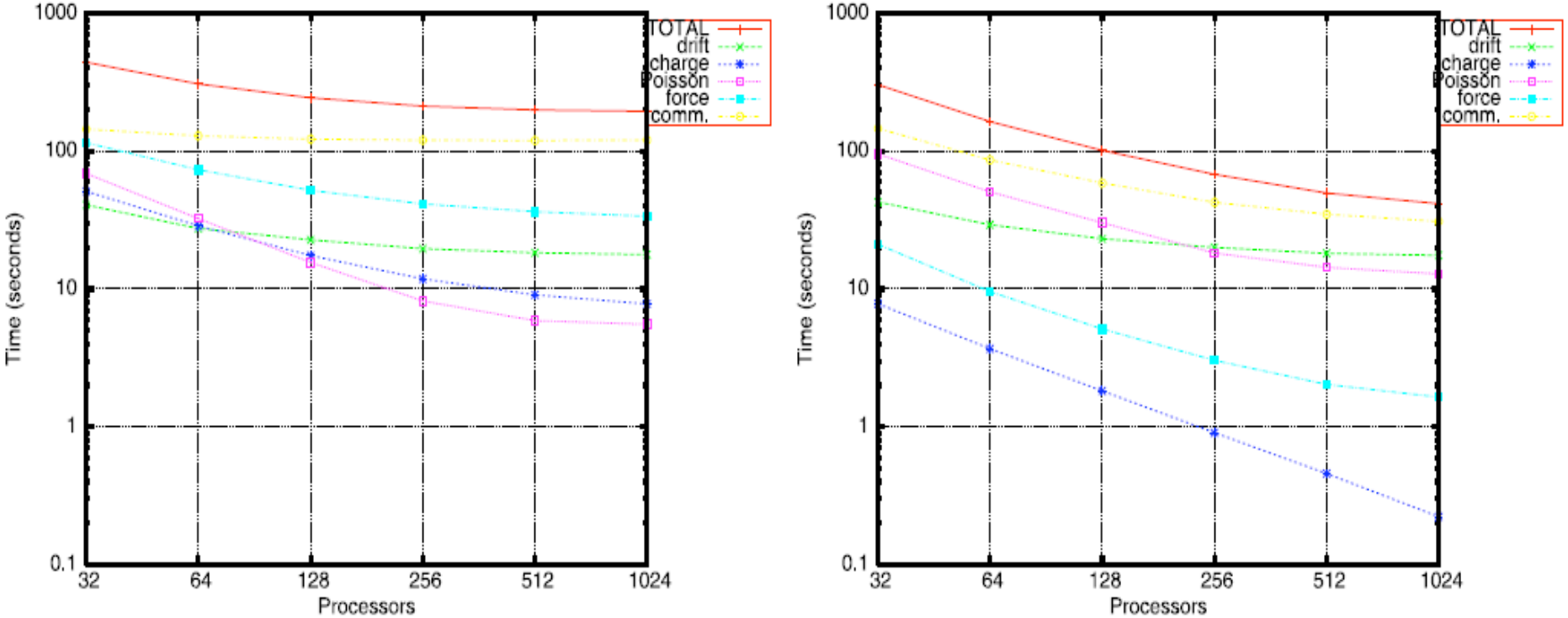

Fig. 6. Computing time as a function of number of processors on Cray XT4 using the particle-field decomposition scheme (left) and the domain decomposition scheme (right) in the strong scaling test B with $128 \times 128 \times 128$ grid points and 10 million particles.

IMPACT – Integrated Map and PArtiCle Tracking

- A 3D parallel multi-physics particle-in-cell code suite
- It includes a "z" dependent and a "t" dependent PIC codes, RMS envelope code, pre and post-processing codes.
- Key Features:
  - Detailed RF accelerating and magnetic focusing model
  - Multiple 3D Poisson solvers
    - Variety of boundary conditions
    - 3D Integrated shifted Green Function
  - Multi-charge state
  - Accelerator machine error model and steering model
  - Wakefields
  - Coherent synchrotron radiation (1D)
  - Monte Carlo gas ionization model

Some Application Examples

LEDA Halo Experiment Channel

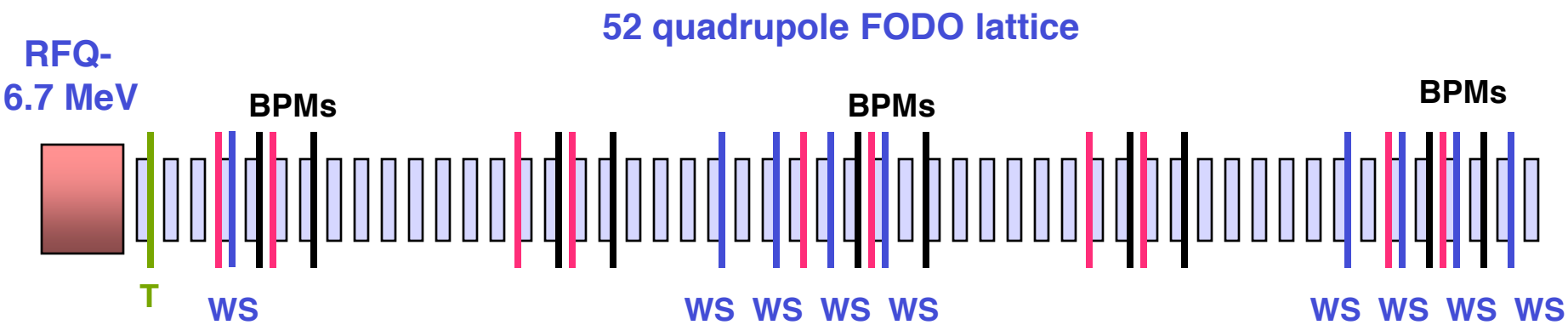

52 Quadrupoles
10 Steering Magnets
9 Wire Scanners
1 Toroid
10 Beam Position Monitors

Courtesy of T. Wangler

Cumulative Density Distribution of Beam in the LEDA (100 M Particle Simulation)

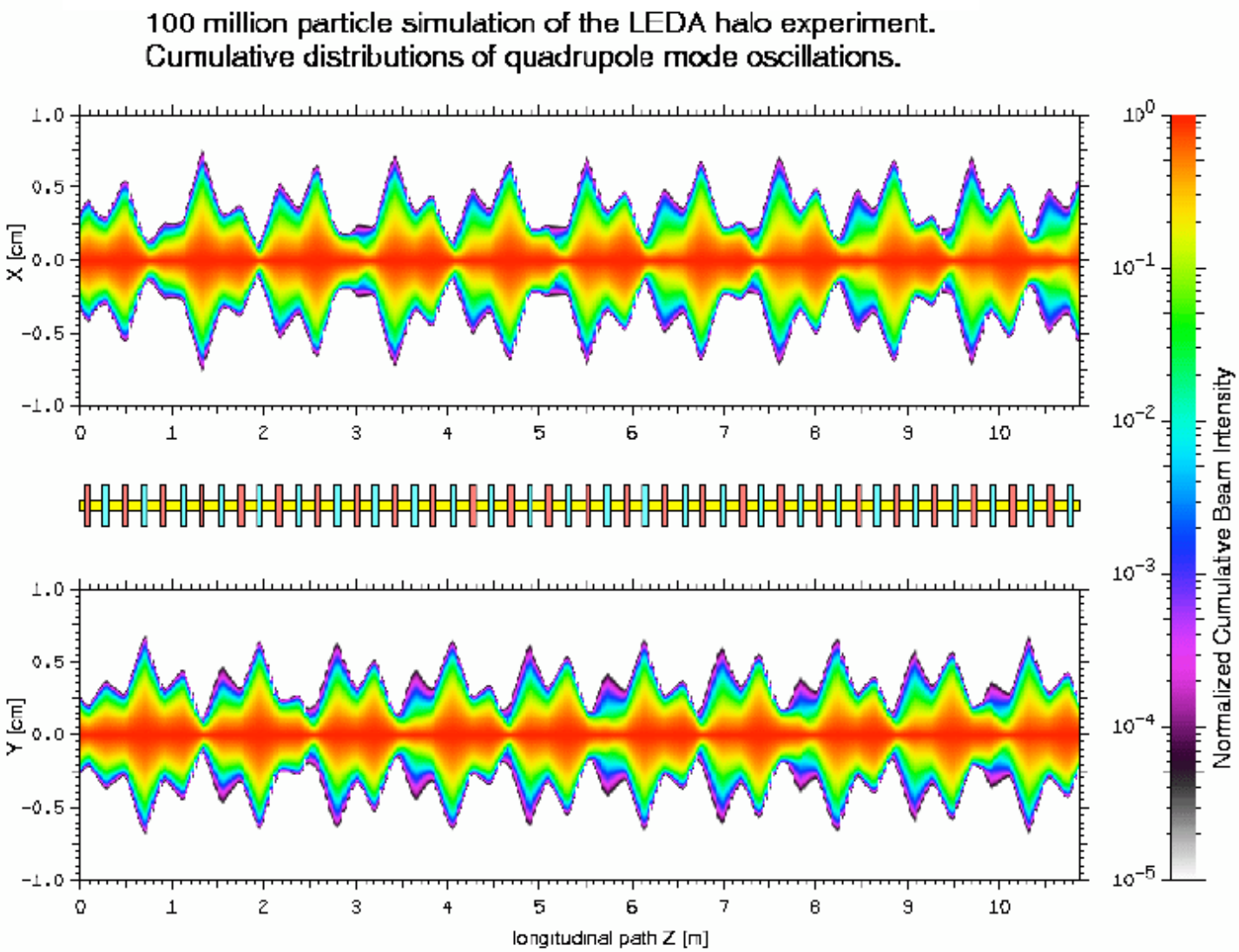

SNS Beam Dynamics Studies: Details of Space-Charge and RF Nonlinearities

IMPACT model and measurement at the MEBT

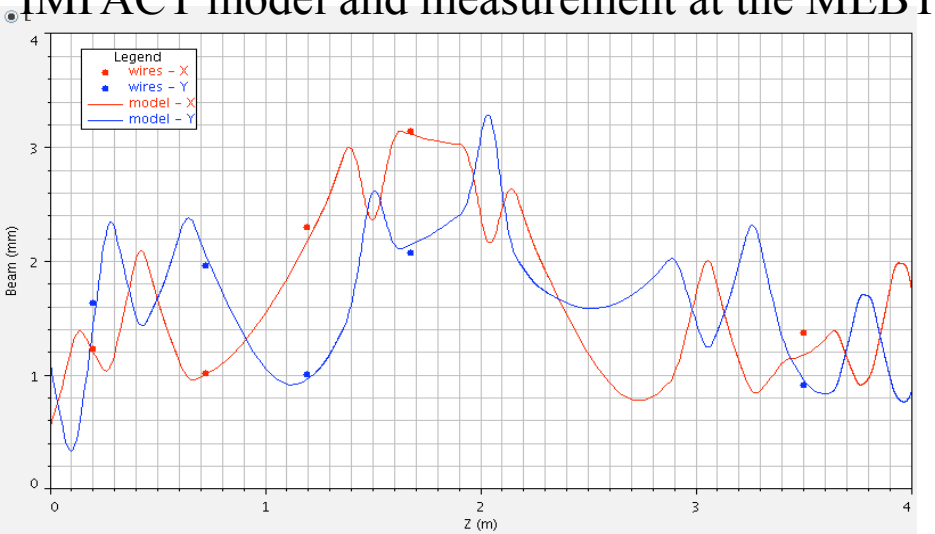

IMPACT model and the LWs measurements in SC linac

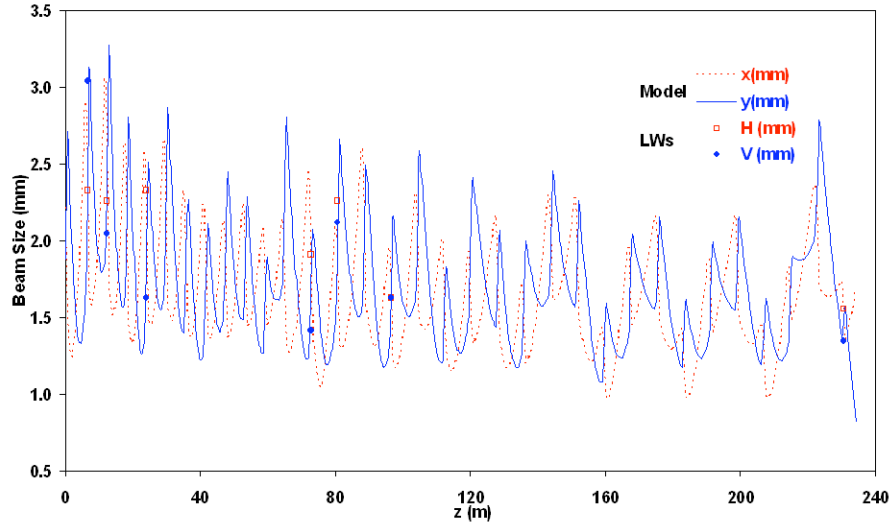

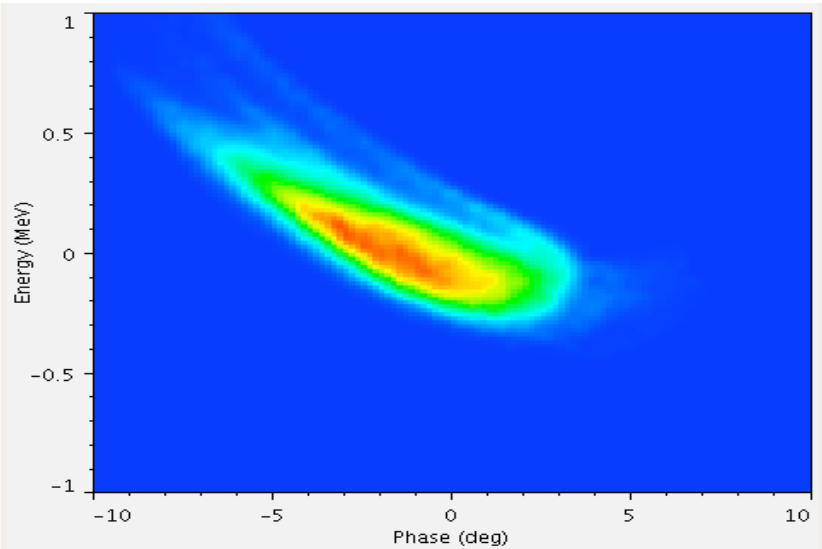

IMPACT model of DTL6 phase shifted by 6°.

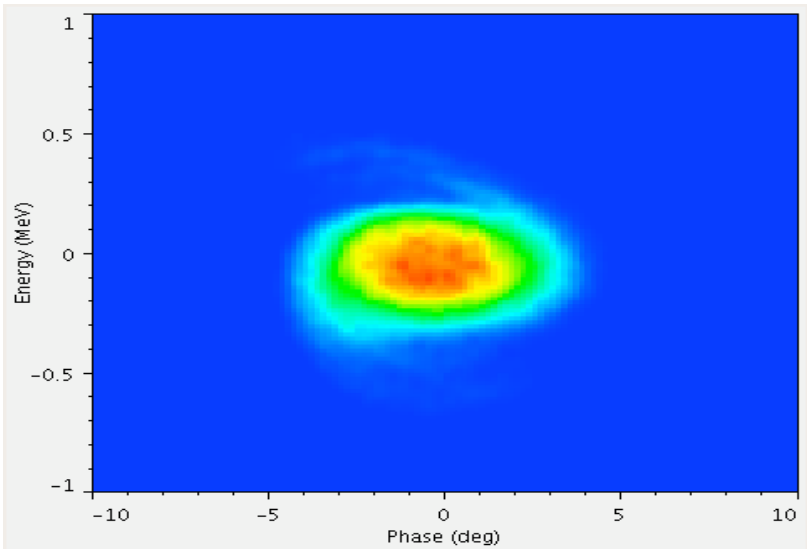

IMPACT predicted profiles at the SCL entrance

Y. Zhang and J. Qiang, PAC09, p. 2653.

Space-Charge Simulation of the PS2

➢PS2 was proposed for LHC upgrade with higher injection energy (4 GeV to mitigate the space-charge effects to reach higher number of protons per bunch (4 x 10^{11}).

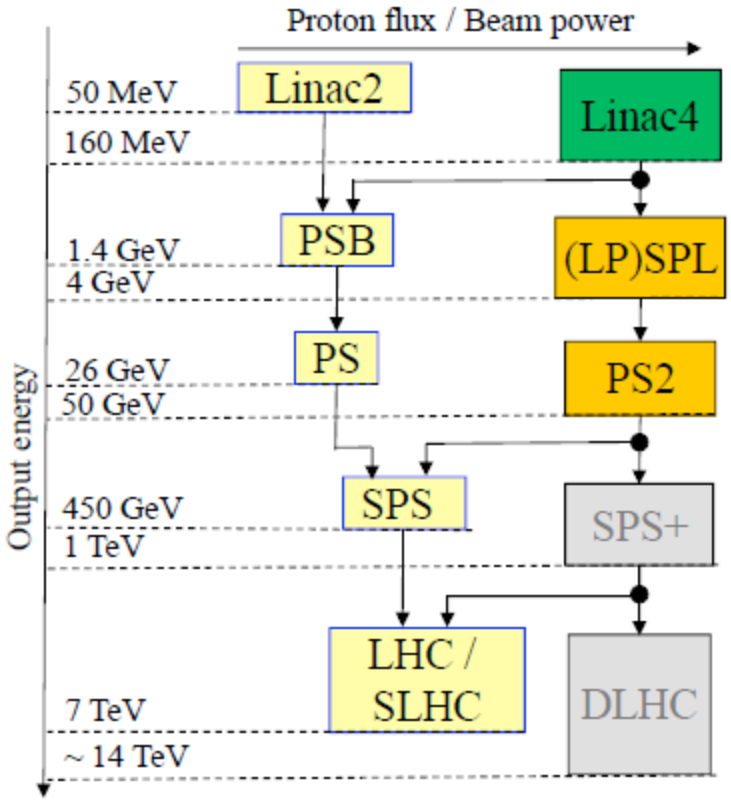

Figure 1: Overview on the CERN injector complex upgrade programme: stage 1 (green), stage 2 (orange).

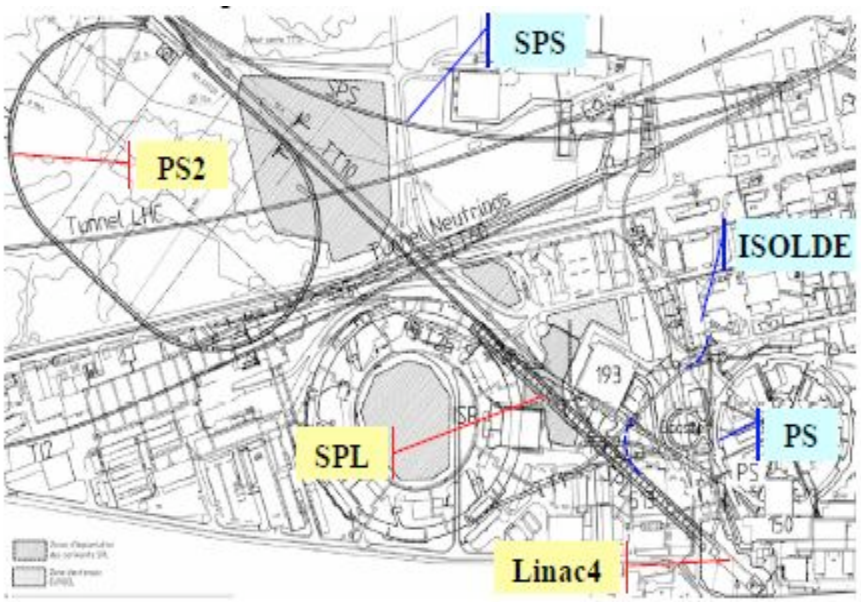

Figure 2: Integration of PS2 within the existing and future CERN accelerator complex.

M. Benedikt, et al., PAC09, WE1GRI03

Goals of PS2 Space-Charge Simulation

- Space-charge effects limit the performance of PS2 by degrading the beam quality, causing halo formation and particle losses
- Fully 3D self-consistent simulation help evaluate the potential dangers of the space-charge effects
- Identify the intensity limit of the space-charge dominated beam
- Optimize the PS2 accelerator design to minimize the space-charge causing beam quality degradation and particle losses

Transverse Emittance Growth with/without Space-Charge Effects

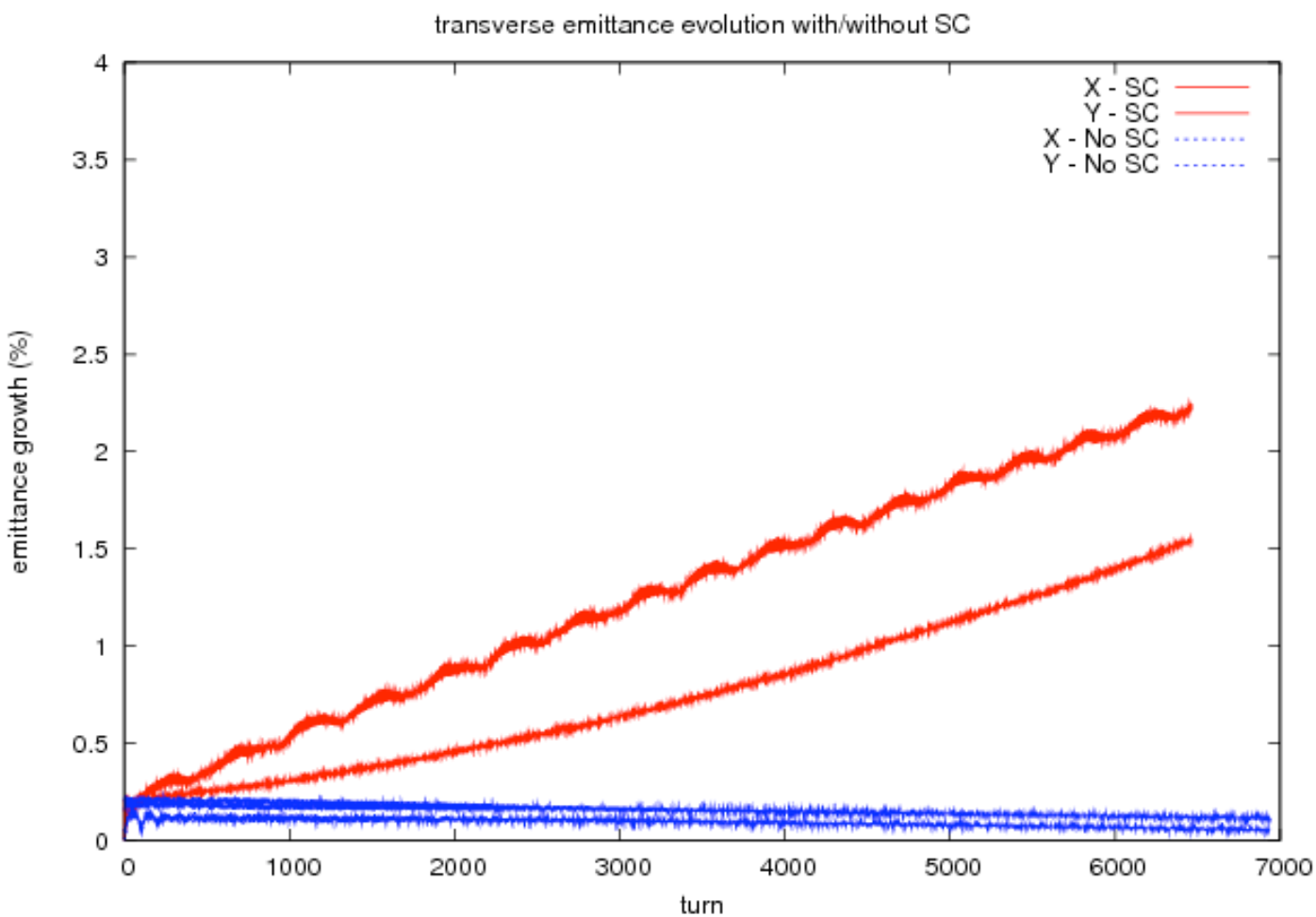

Betatron Tune Footprint with 0 Current and with SC but no Synchroton Motion

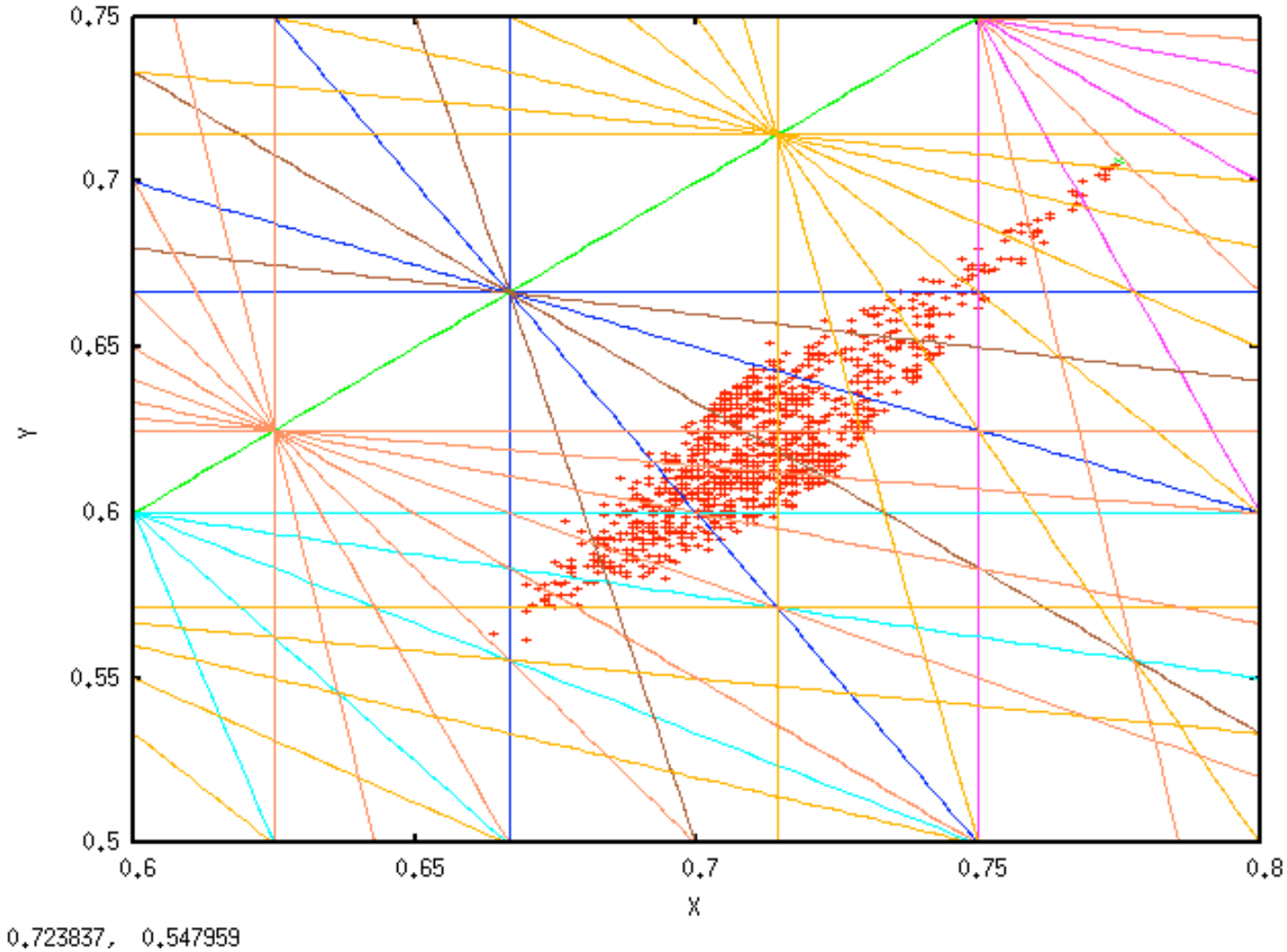

Betatron Tune Footprint with 0 Current and with SC and Synchroton Motion

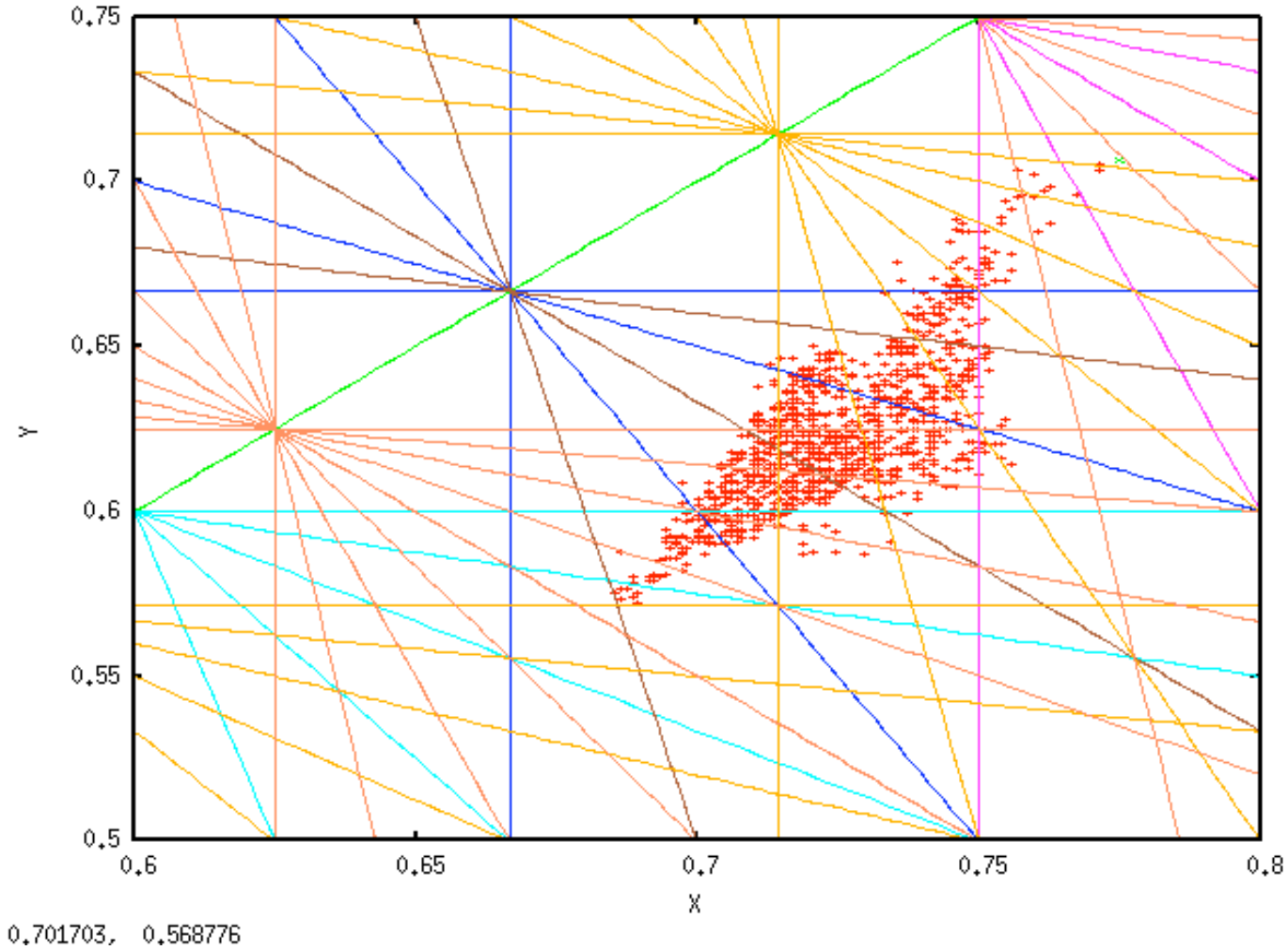

Transverse Emittance Growth with/without Synchrotron Motion

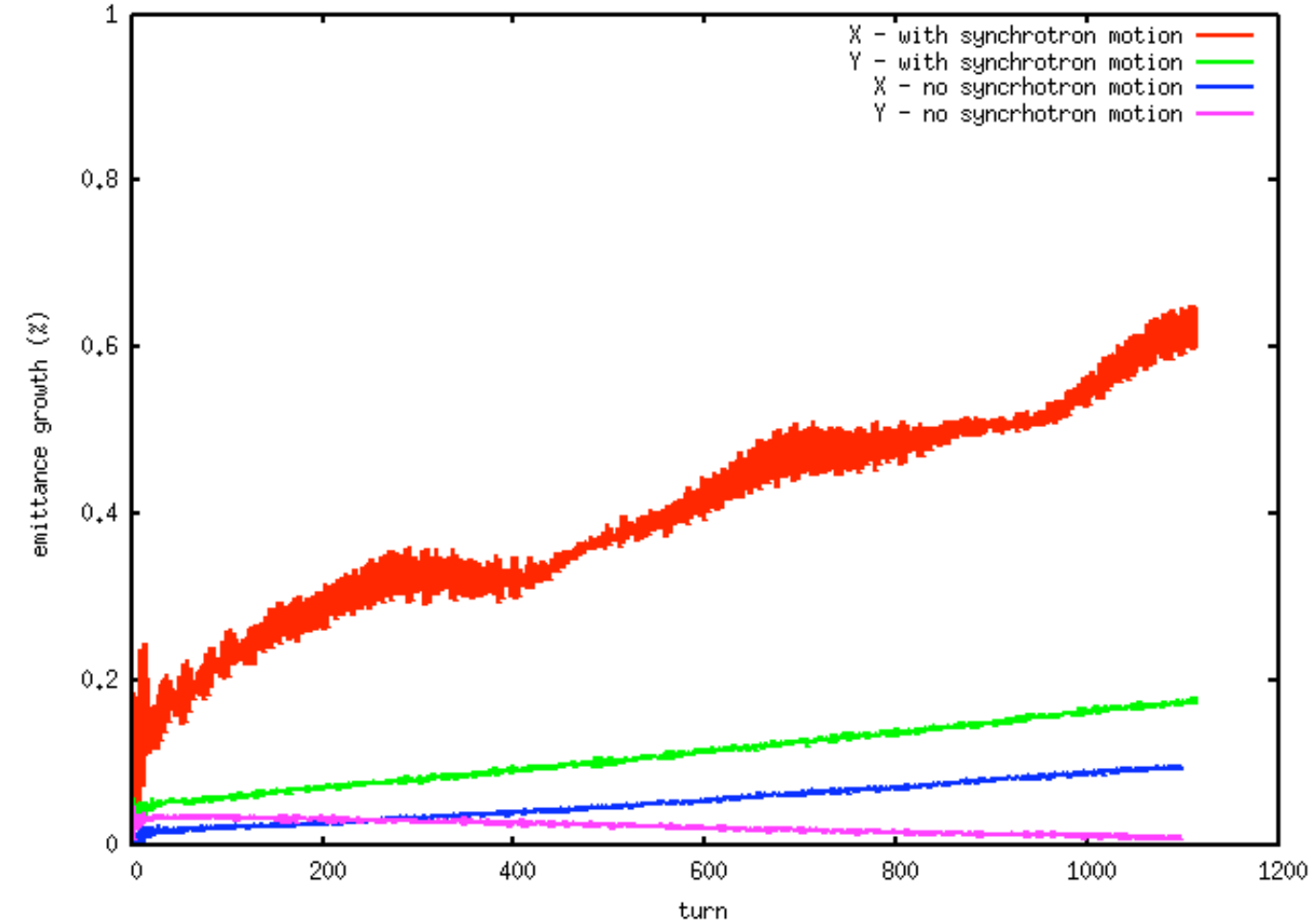

-134.756, -0.0938776

Vision for a future light source facility at LBNL

A HIGH REP-RATE, SEEDED, VUV — SOFT X-RAY FEL ARRAY

FEL Power/ undulator length $\sim f\left(I_{peak}, \frac{\varepsilon_n}{\gamma}, \sigma_E\right)$

Array of configurable FELs

- Independent control of wavelength, pulse duration, polarization
- Configured with an optical manipulation technique; seeded, attosecond, ESASE

Beam manipulation and conditioning

Beam distribution and individual beamline tuning

~2 GeV CW superconducting linac

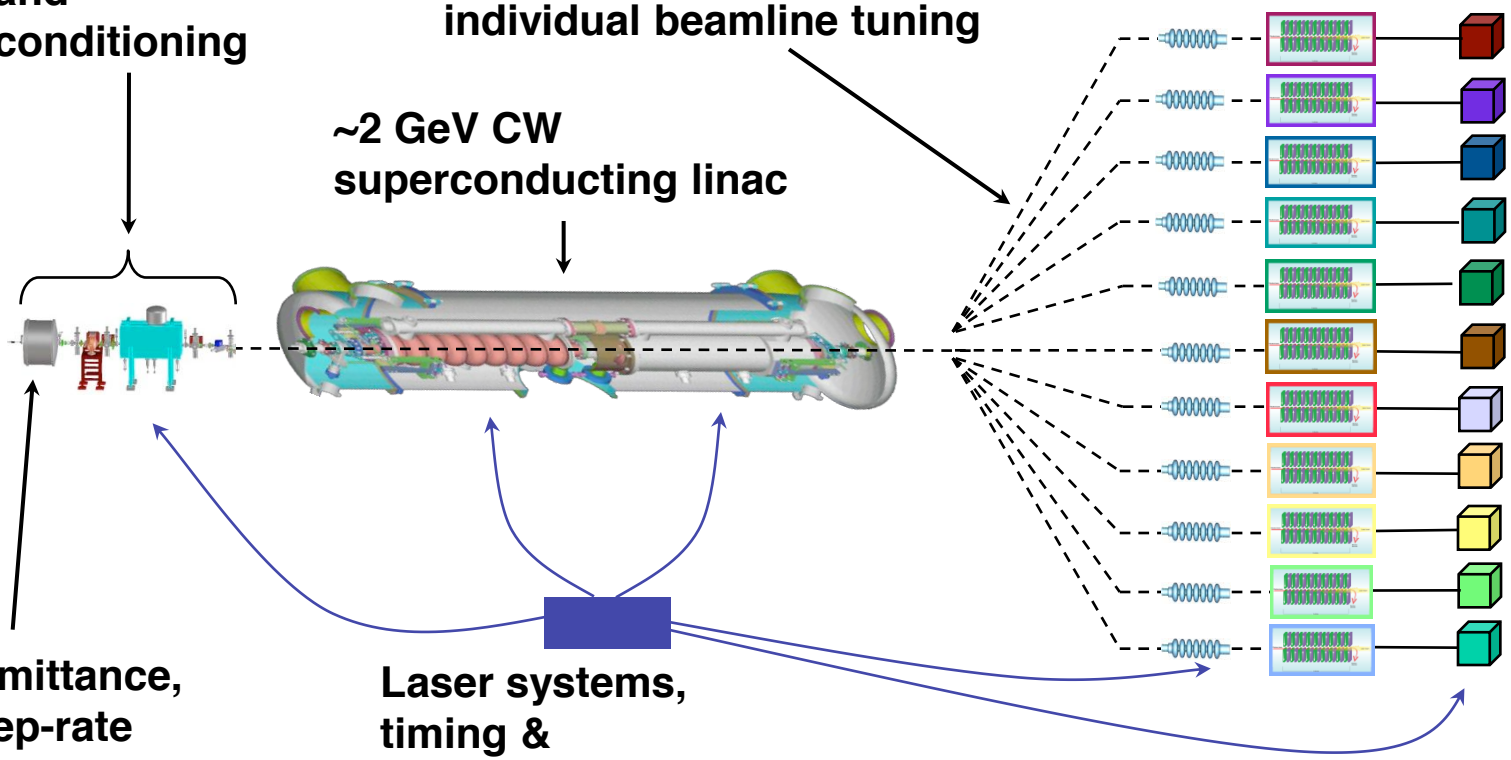

Low-emittance, high rep-rate electron gun

Laser systems, timing & synchronization

Courtesy of J. Corlett

Space-Charge Driven Energy Modulation vs. Distance (Simulation vs. Analytical Models)

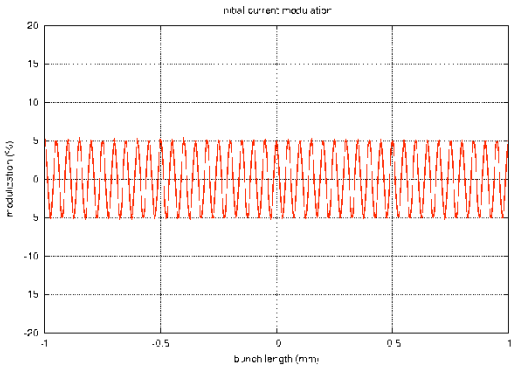

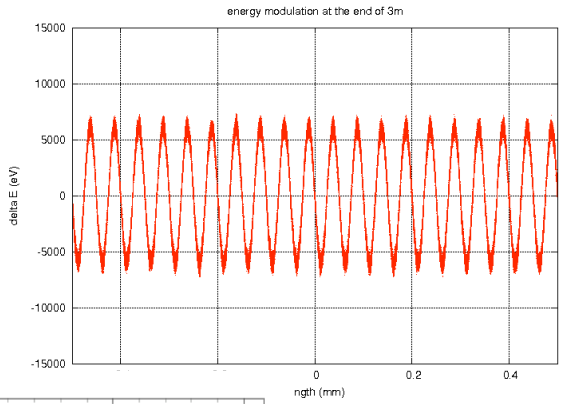

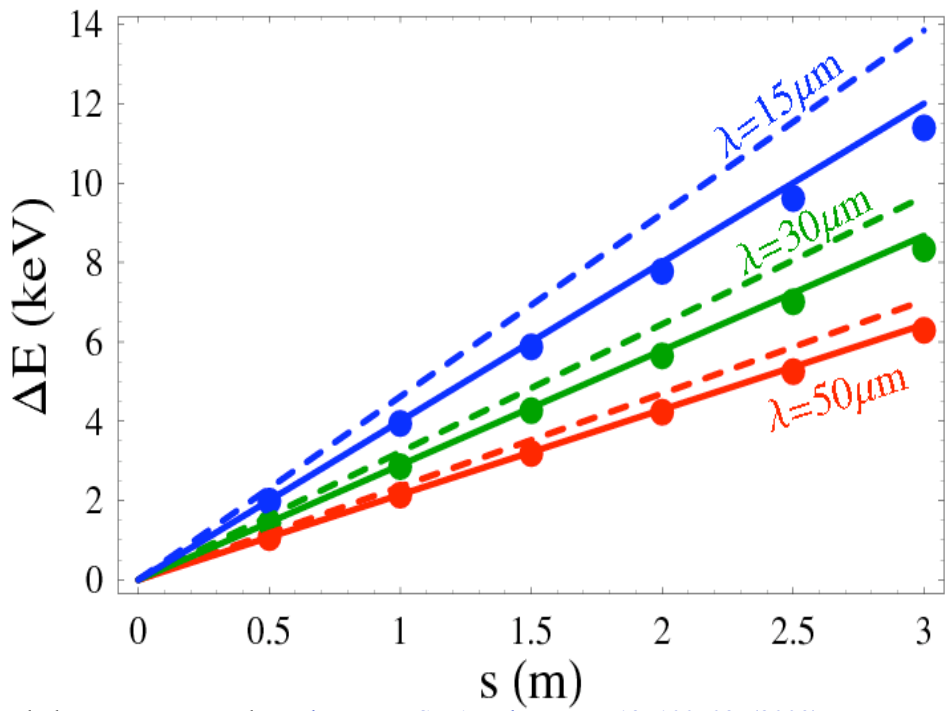

J. Qiang, R. D. Ryne, M. Venturini, A. A. Zholents, I. V. Pogorelov, Phys. Rev. ST Accel. Beams, 12, 100702 (2009).

Microbunching Instability Gain Curve

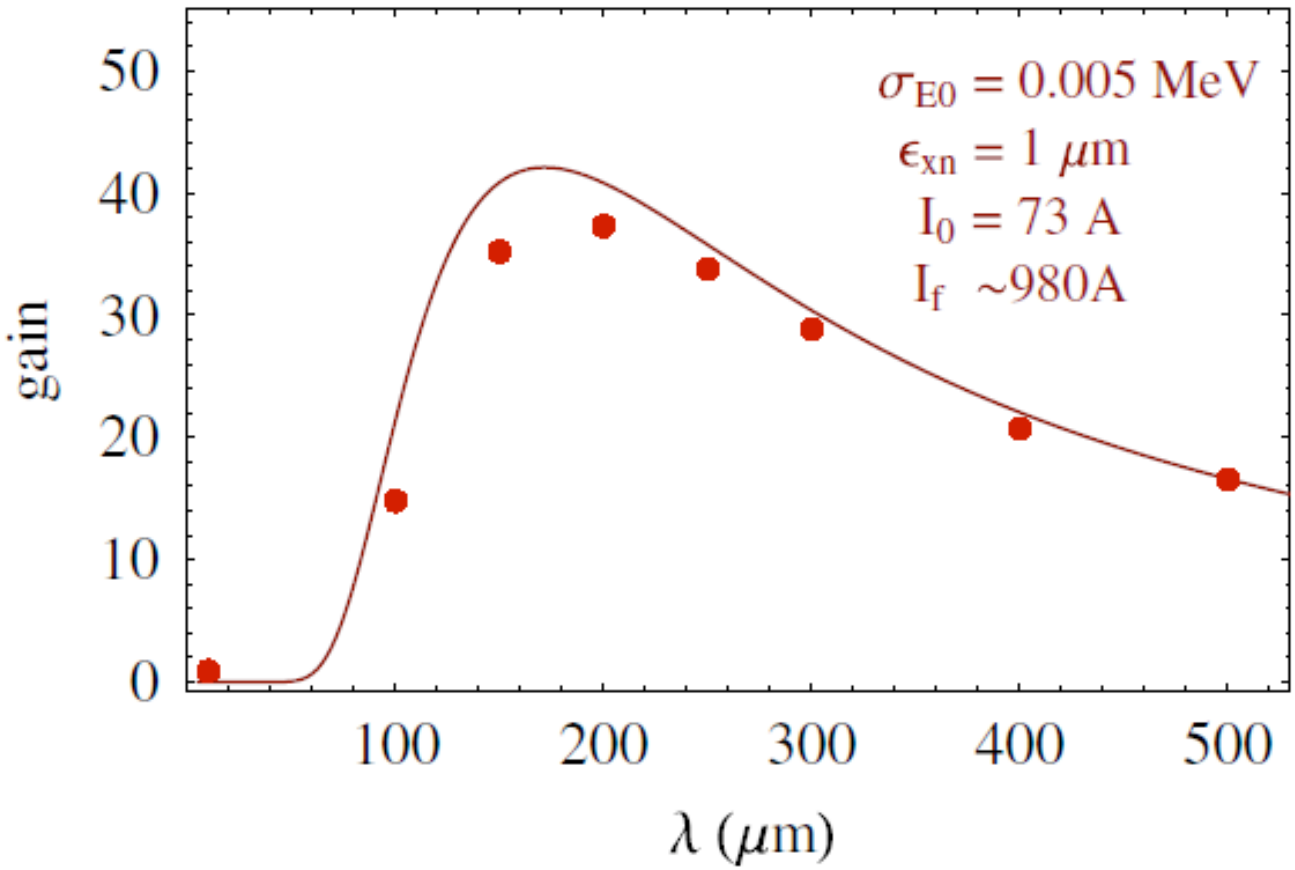

Final Uncorrelated Energy Spread vs. Number of Macroparticles

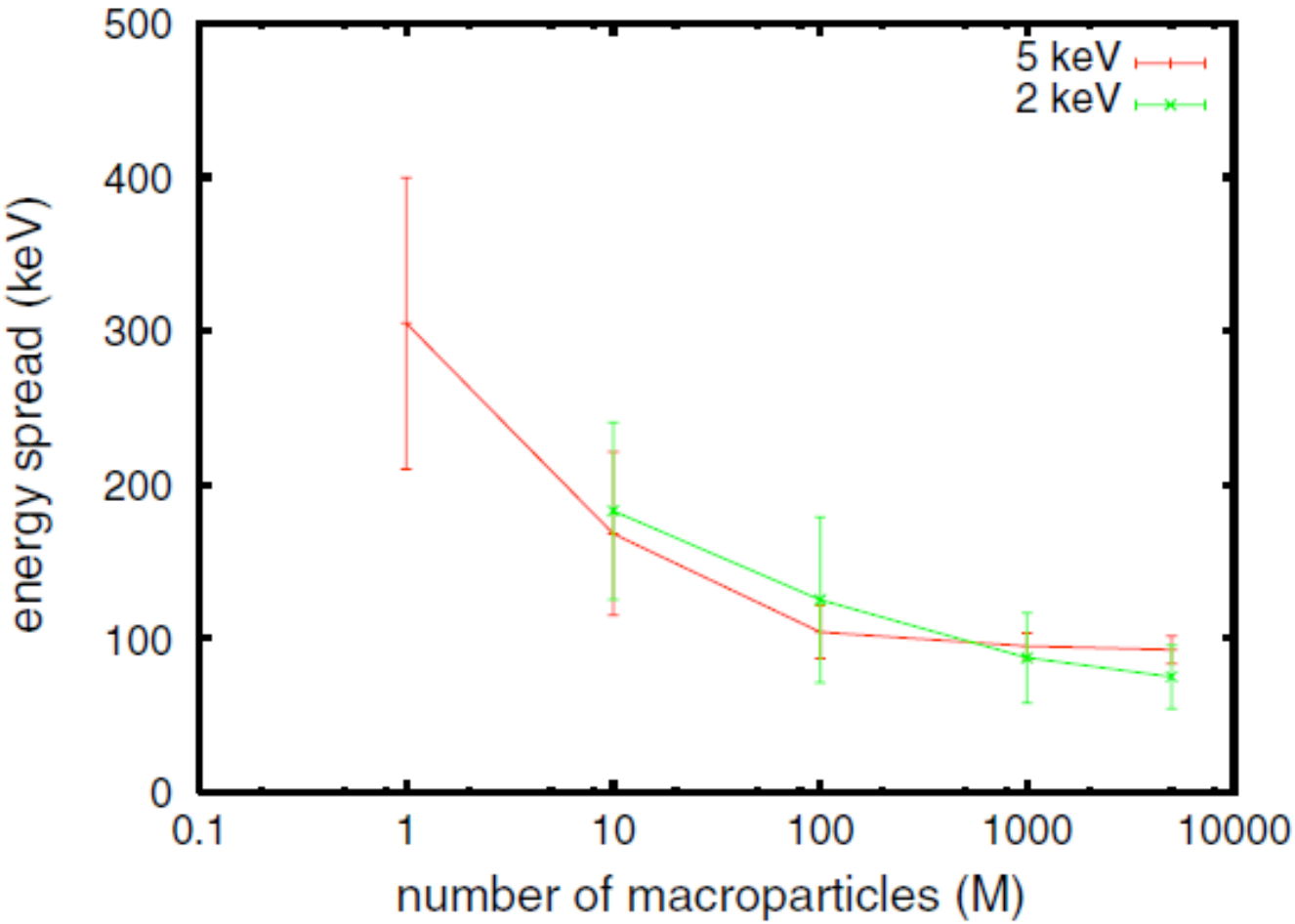

Final Uncorrelated Energy Spread vs. Initial Energy Spread

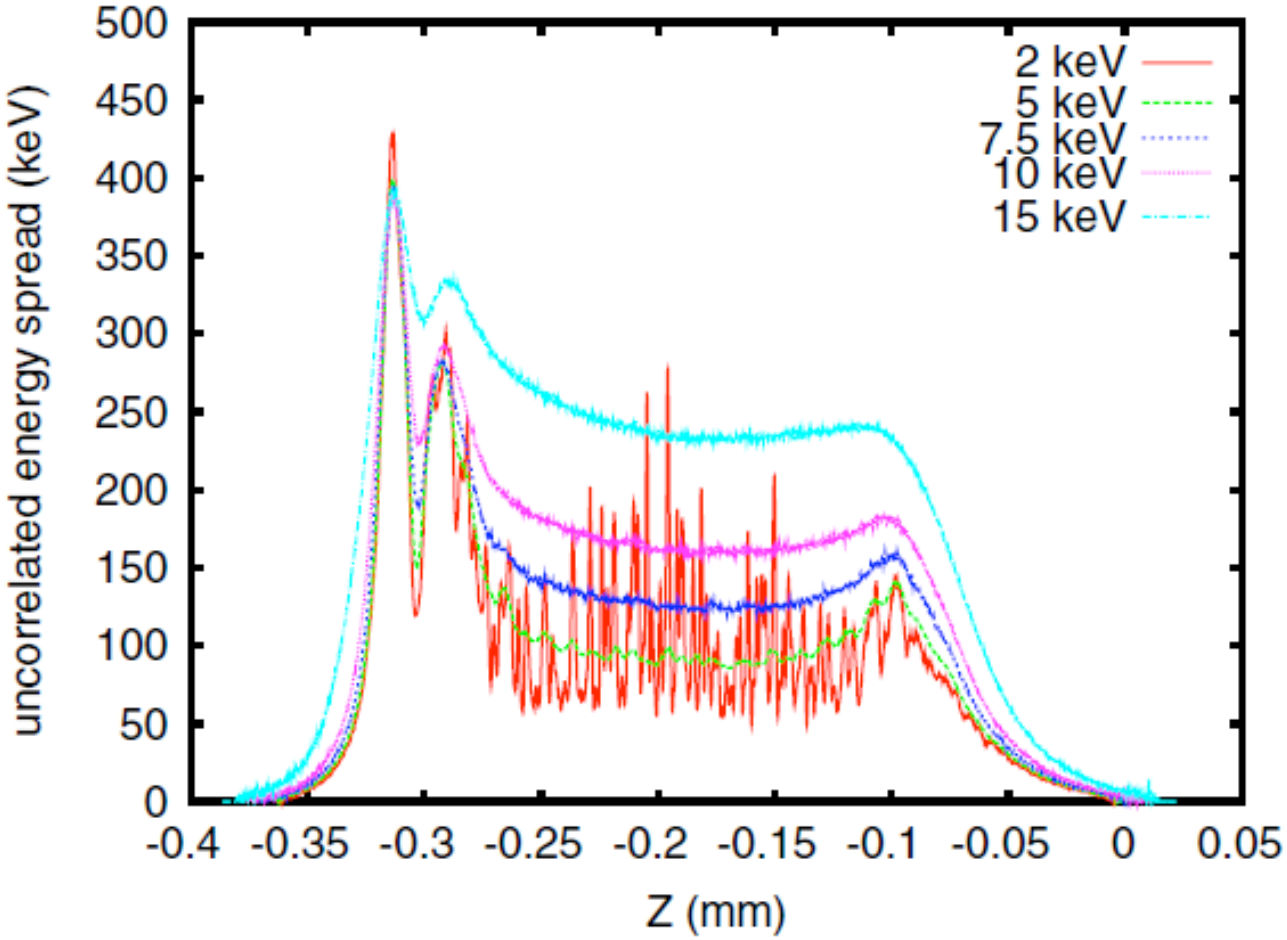

Final Longitudinal Phase Space Distribution with One and Five Billion Macroparticles

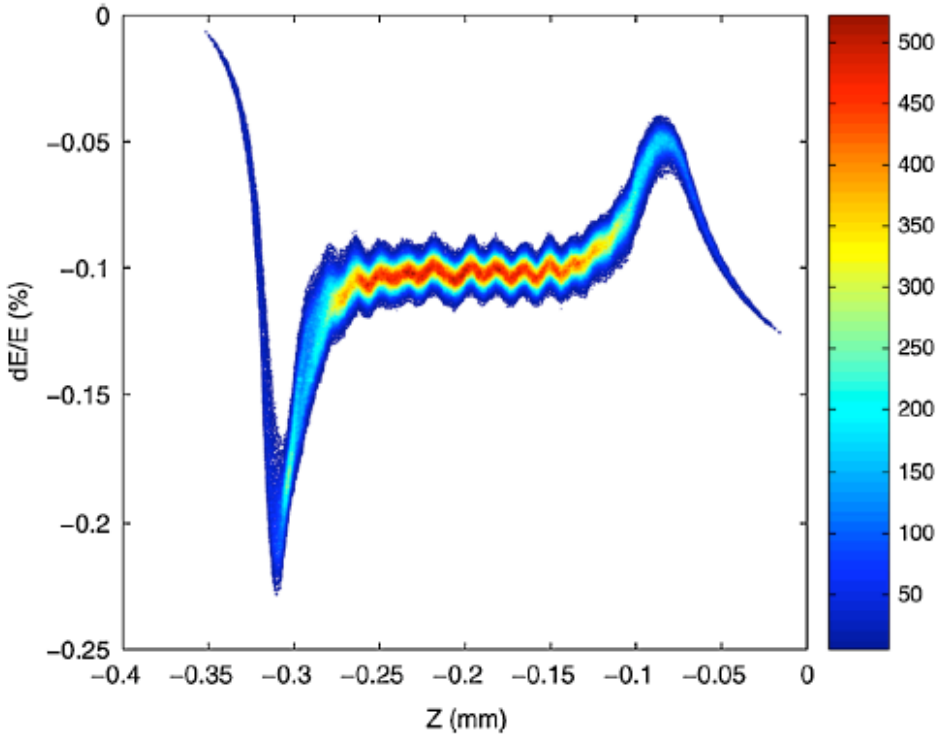

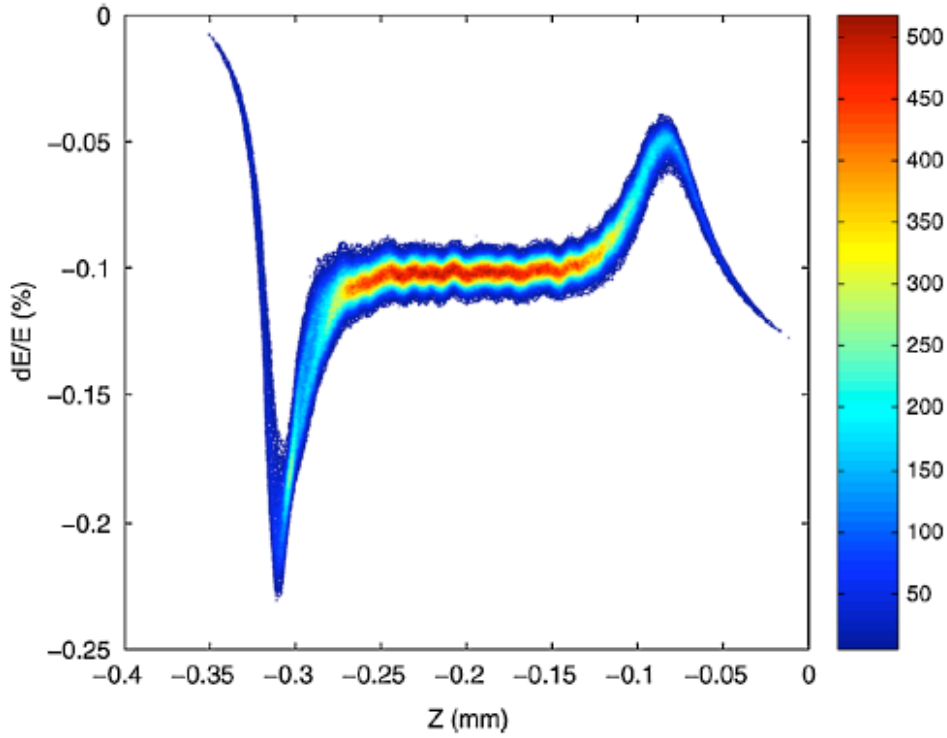

Acknowledgements:

J. Corlett, V. Decyk, M. Furman, R. Gluckstern, I. Hofmann, X. Li, R. Ryne, M. Venturini, T. Wangler, A. Zholents, Y. Zhang, and many other collaborators.

Work supported by the Office of Science of the U.S. Department of Energy under Contract No. DE-AC02-05CH11231.

Thank you!